Phase formation behaviour in alkali activation of clay mixtures

Marsh, A.[1]; Heath, A. [1]; Patureau, P. [2]; Evernden, M. [1]; Walker, P. [1]

[1] Department of Architecture & Civil Engineering, University of Bath, Bath, BA2 7AY, United Kingdom

[2] Department of Chemistry, University of Bath, Bath, BA2 7AY, United Kingdom

https://doi.org/10.1016/j.clay.2019.03.037

Abstract

Alkali-activated soils have potential as low carbon, low cost construction materials. There is a lack of fundamental understanding around how soil composition influences alkali activation behaviour, especially for uncalcined soils. The types and relative amounts of clay minerals can vary greatly throughout soils across the world. Since clays are typically the dominant reactive aluminosilicate constituent in soils, it is desirable to understand how the types and relative amounts of clay minerals influence reaction products in alkali activation. In this study, mixtures of kaolinite, montmorillonite and illite precursors were activated with sodium hydroxide solutions. By comparing with extrapolations of cross-characterisation from the behaviour of individual clays, it was shown that phase formation behaviour deviated from an ideal rule of mixtures model. Instead, there was a hierarchy between the clays in determining the reaction products: kaolinite and montmorillonite dominated illite in this regard. This study demonstrates that the viability of a given soil for alkali activation depends not only on the total amount of clay, but the types and relative amounts of clay minerals present. In order to unlock the potential of alkali-activated soils, more understanding is needed of the role of the different components in soil.

Highlights

- Hierarchy of clays in reactivity and determining product phases formed
- Rule of mixtures model does not fully describe alkali activation behaviour
- Change in Si-O-T FTIR band position indicates product phases

Graphical abstract

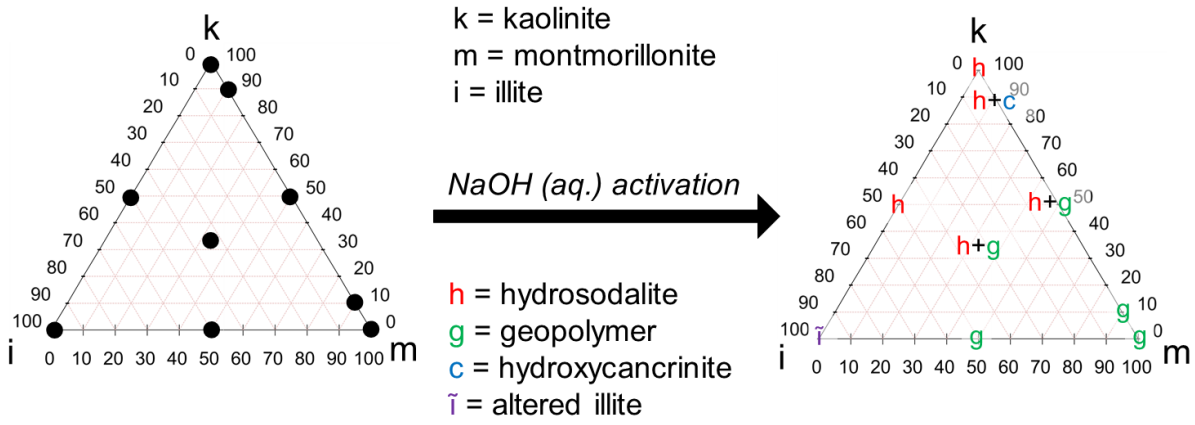

1 Introduction

Alkali-activated materials are a promising candidate for low carbon construction materials (Davidovits, 2011; Provis, 2014). The principle of alkali activation is to transform an aluminosilicate precursor into an alkali aluminosilicate phase by the addition of an alkaline activating solution, followed by mixing and curing (Duxson et al., 2007a). The exact alkali aluminosilicate phase produced in this reaction depends on several compositional and processing factors - most importantly, the Si:Al ratio of the dissolved precursor (Duxson et al., 2007b; Weng and Sagoe-Crentsil, 2007). It is usually intended to form an amorphous gel phase, also known as a geopolymer, as this possesses good strength, durability and other desirable properties (Liew et al., 2016). It is also possible to form crystalline products, typically members of the zeolite family (Criado et al., 2007). Crystalline products are more likely to form at lower Si:Al ratios while geopolymer phases are more likely to form at higher Si:Al ratios (Buchwald et al., 2011; Duxson et al., 2007b), as discussed later.

Within the family of alkali-activated materials, alkali-activated soils have significant potential because subsoil is a widely available natural resource, available at very low environmental cost (Diop and Grutzeck, 2008). Subsoil is also a waste stream - soils typically make up the single largest component of construction waste (Llatas, 2011). In the application of soil stabilisation for construction blocks, the alkali aluminosilicate product fulfils the function of the stabilising phase (Murmu and Patel, 2018). By being stronger and less expandable than the clay mineral precursors it replaces, it improves the strength and durability of the soil. However, a significant barrier to adoption is a lack of understanding of how soil composition influences the alkali activation reaction.

Soils are composed of clay minerals, unreactive quartz, and other associated minerals typically in minor quantities (Dixon and Weed, 1989). The most common clay minerals in soils are kaolinite, montmorillonite and illite, with allophane and halloysite less common (Reeves et al., 2006). The dissolution of aluminosilicates in a concentrated alkaline solution determines the ultimate extent of alkali aluminosilicate phase formation (Xu and Van Deventer, 2000). Of the aluminosilicate phases in soils, clays are typically the most soluble component, more so than other common

minerals such as quartz (Autef et al., 2012; Tchakoute et al., 2015) and muscovite (Zografou, 2015).

Previous studies have investigated the effect of aluminosilicate precursor and activating solution composition on geopolymer formation (Pacheco-Torgal et al., 2008). However, this is generally done using an aluminosilicate precursor of roughly fixed stoichiometric composition (usually metakaolin) and varying the chemical ratio of the liquor by adding additional soluble Si (Duxson et al., 2007b; Duxson et al., 2005). This is not the same as supplying silicates solely from mineral precursors, as such minerals' behaviours are likely to differ based on dissolution rates (Bauer and Berger, 1998; Xu and Van Deventer, 2000) and particle size effects (Weng et al., 2005). Although it is well-established that clays are more reactive when calcined, the energy cost of this step gives a strong incentive to investigate the activation of un-calcined clays (MacKenzie, 2009).

The alkali activation behaviour of individual clay minerals kaolinite (Liew et al., 2016), montmorillonite (Belviso et al., 2017; Seiffarth et al., 2013) and illite (Belviso et al., 2017; El Hafid and Hajjaji, 2015; Seiffarth et al., 2013; Sperberga et al., 2011) have previously been investigated. However, almost all previous studies on montmorillonite and illite have used their calcined state. Non-kaolinitic calcined clays have been used as supplementary cementitious materials in Portland cement blends (Hollanders et al., 2016; Snellings et al., 2012; Tironi et al., 2013). However, these studies involve high-Ca environments in order to form C-S-H phases, and so have limited transferability to low-Ca environments where the objective is to form N-A-S-H geopolymers. Whilst kaolinite (Liew et al., 2016), real soils (Lemougna et al., 2014), and blends of uncalcined real soils and other materials such as metakaolin (Omar Sore et al., 2018) are popular for studies, there has been much less attention on the alkali activation of individual clays, and in particular, controlled mixtures of clays. Soils around the world contain clays in different amounts (Abe et al., 2006; Nickovic et al., 2012), notwithstanding other minor minerals. Improving our fundamental understanding of how mixtures of clays react under alkali conditions is crucial to determining whether alkali-activated soils can be widely used and reliable construction materials.

Few previous studies have used a systematic approach for understanding the alkali activation behaviour of clay mixtures. Richardson et al. (1986) showed that binary and ternary mixtures of kaolinite, montmorillonite and illite activated using aqueous NaOH solution produced reaction products of combinations of sodalite, cancrinite and nepheline. However, no mention of geopolymers or amorphous phases was made, and since only XRD characterisation was used, this gives an incomplete picture of the activated systems. In addition, very short curing times (less than 30 minutes) microwave curing was used, giving limited comparability with other systems. Buchwald et al. (2011) showed that for solutions of aluminium and silicon, geopolymer formation was favoured for systems with Si:Al > 1.5, with geopolymers and zeolites co-existing in some systems. This is a valuable contribution to fundamental understanding, but there is still a gap to consider the effects of mineralogy and composition of natural aluminosilicate precursors.

In this study, a Rule of Mixtures (RoM) approach was used to investigate how phase formation behaviour in alkali activation differed for mixtures of clays, compared to the activation of the constituent clays individually. The RoM approach has been used to evaluate a range of properties for material mixtures including elastic modulus (Marom et al., 1978) and glass transition temperature (Couchman, 1978), as well as to evaluate phase formation in material mixtures (Donald and Davies, 1978). Mixtures of the common clay minerals kaolinite, montmorillonite and illite were activated with NaOH solutions, in order to determine their phase formation behaviour in comparison with the clays as individuals.

2 Experimental

2.1 Materials

Imerys Speswhite kaolin (mined from Cornwall, U.K.), K10 montmorillonite (Sigma-Aldrich, product no. 69866-1KG) and Clay Minerals Society IMt-2 (Silver Hill) illite were used as the precursor clays. Chemical compositions were determined by energy dispersive X-rays (JEOL SEM6480LV with Oxford INCA X-Act SDD X-ray detector), and specific surface area was measured using the BET method (Brunauer et al., 1938) using a Micromeritics 3-Flex.

The kaolinite (Kao), montmorillonite (Mont) and illite (ILL) precursor clays have previously been characterised (Marsh et al., 2018a; Marsh et al., 2018b), but will

briefly be restated here. The XRD pattern of the kaolinite precursor gave kaolinite clay mineral as the major phase, with muscovite and quartz present as minor phases (Figure 1), as expected from a Cornish mixed hydrothermal and residual deposit (Murray and Keller, 1993). The XRD pattern of the montmorillonite precursor showed it contained montmorillonite clay mineral as the major phase, along with muscovite, quartz and minor amounts of feldspar and kaolinite (Figure 1). The refined basal spacing of 14.4 Å suggested it was a Ca-montmorillonite (Ferrage et al., 2005). The XRD pattern of the illite showed it contained illite clay mineral as the major phase, with quartz, microcline and kaolinite present as minor phases (Gailhanou et al., 2007) (Figure 1). Previous studies on this source clay identified the illite clay mineral to be mostly of the 1M/1Md polytype (Haines and van der Pluijm, 2008).

The kaolinite precursor contained minor amounts of iron, potassium and magnesium (Table 1) and these were not considered to have a major effect on the reactions and products under the conditions in this study. BET specific surface area was 11.9 m^2g^{-1}. The montmorillonite precursor contained minor amounts of iron, potassium, magnesium, sodium, sulphur and titanium (Table 1). BET specific surface area was 265.8 m^2g^{-1}. The illite precursor contained minor amounts of iron, potassium, magnesium and titanium (Table 1). BET specific surface area was 19.5 m^2g^{-1}.

The precursor clays were activated using sodium hydroxide pellets of >98% purity (Sigma-Aldrich, product no. 06203).

Table 1: Chemical composition of clay precursors in oxide wt%, after LOI removed.

Oxide (wt.%)	Al_2O_3	CaO	Fe_2O_3	K_2O	MgO	Na_2O	SiO_2	SO_3	TiO_2	Total
Speswhite kaolin (std error)	40.11 (0.15)	0.00	0.95 (0.06)	2.06 (0.09)	0.04 (0.04)	0.00	56.83 (0.15)	0.00	0.00	100
K10 Montmorillonite (std error)	13.53 (0.66)	0.47 (0.14)	4.53 (1.05)	1.56 (0.22)	1.67 (0.11)	0.03 (0.03)	77.60 (2.12)	0.12 (0.07)	0.49 (0.02)	100
IMt-2 illite (std error)	20.80 (0.34)	0.00	8.32 (0.38)	8.67 (0.18)	2.28 (0.06)	0.00	59.14 (0.26)	0.00	0.78 (0.06)	100

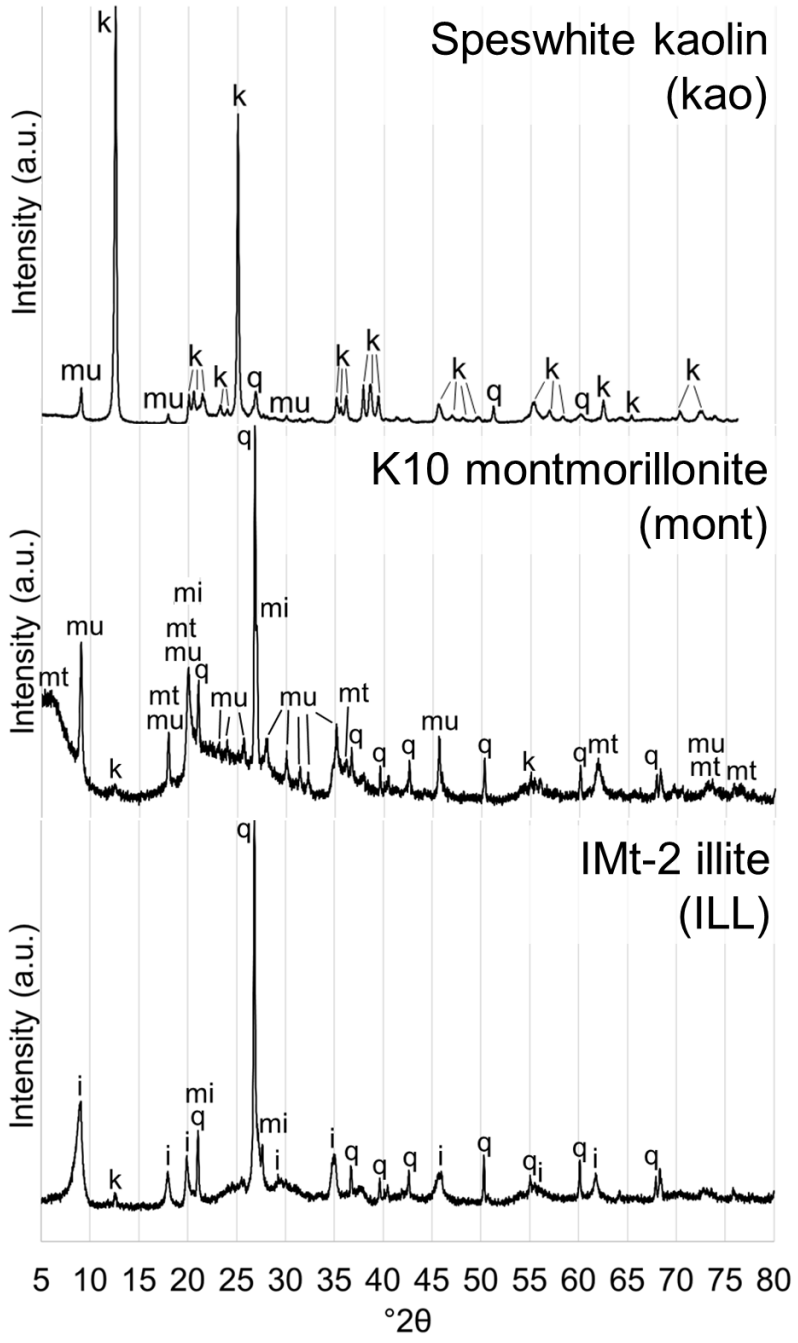

Figure 1: XRD patterns of the clay precursors.

2.2 Synthesis procedure

Using the same procedure as used in a previous study (Marsh et al., 2018b), the masses of clays, water and NaOH for each sample (Table 2) were specified so that all samples had two characteristics. Firstly, all samples had the same Na:Al molar ratio (chosen to be 1), and secondly, the wet mix consistency of all samples was at

the plastic limit. This was done by initially undertaking Atterberg plastic limit measurements (Wagner, 2013) for the clay minerals over a range of sodium hydroxide solutions. The exception to this condition is activated illite – due to its lower plastic limit, the maximum Na:Al molar ratio that could be achieved was 0.75 without exceeding the saturation limit of $NaOH_{(aq.)}$ at room temperature. The plastic limits of the clay mixtures were estimated from the plastic limit behaviour of the individual clays. This was done by summing the plastic limit of each constituent clay for a given NaOH concentration, factored by the relative fraction of that clay in the mixture. This workability constraint was chosen in order to make the wet mixes compatible with extrusion, an established brickmaking process (Maskell et al., 2013), and builds on previous experiments on the alkali activation of individual clays using the same constraints (Marsh et al., 2018a).

Table 2: Compositions of the clay mixtures made in each series. Clay contents given in wt%.

Series	Sample	Kao.Content (%mass)	Mont.Content (%mass)	ILL content (%mass)	[NaOH] molarity	NaOH solution : clay mass ratio
Kao-Mont	100Kao-0Mont	100%	n/a	n/a	16.1	0.73
	90Kao-10Mont	90%	10%	n/a	15.0	0.73
	50Kao-50Mont	50%	50%	n/a	10.7	0.75
	10Kao-90Mont	10%	90%	n/a	7.2	0.77
	0Kao-100Mont	0%	100%	n/a	6.4	0.77
Mont-ILL	100Mont-0ILL	n/a	100%	0%	6.4	0.77
	50Mont-50ILL	n/a	50%	50%	12.2	0.61
	0Mont-100ILL	n/a	0%	100%	19.7	0.39
ILL-Kao	100ILL-0Kao	0%	n/a	100%	19.7	0.39
	50ILL-50Kao	50%	n/a	50%	18.9	0.59
	0ILL-100Kao	100%	n/a	0%	16.1	0.73
Kao-Mont-ILL	33Kao-33Mont-33ILL	33%	33%	33%	13.6	0.65

The chosen combinations of clay mixtures were activated by adding a sodium hydroxide solution. Solutions of different concentrations were prepared by adding sodium hydroxide pellets to distilled water, mixed with a magnetic stirrer (Stuart UC152 heat-stir) for a minimum of 2 h until fully dissolved and then allowed to cool. The clays were pre-dried in a 105°C oven, and left to cool. The constituent clays were then dry-mixed together using the magnetic stirrer for 5 minutes. Varying amounts of activating solutions were added in the quantities presented in Table 2. Each wet mixture of activating solution and clay mixture was mixed by hand for 3 min, providing a consistent and well-distributed mixture. The consistency of the samples allowed them to be compacted by hand into 18 mm x 36 mm cylindrical Teflon moulds by tamping with a glass rod in three layers for each sample, using 25 blows for each layer. Samples were cured in an air atmosphere in an 80°C oven for 24 h in their moulds. For each composition, a control sample was made in addition to an activated sample. Distilled water was used instead of sodium hydroxide solution, such that the consistency of the wet mix was still at the plastic limit. The control samples were then mixed and cured in the same manner as the activated samples.

Samples 50Kao-50Mont, 50ILL-50Kao and 33Kao-33Mont-33ILL did not fully dry with curing, so were forcibly dried in a vacuum desiccator for 72 h. After demoulding, samples were aged for 28 days in a controlled environment of 20 ± 0.5°C and 50 ± 2.5% relative humidity. An air atmosphere was intentionally used for both curing and ageing, to provide conditions representative of industrial brickmaking processes.

2.3 Characterisation methods

The set of characterisations were done at 28 ± 2 days ageing time, and (with the exception of SEM imaging) were performed on powders prepared from the cured samples. These were ground by hand, having been wetted with isopropanol to avoid damaging the clay mineral crystal structures (Moore and Reynolds, 1997). For XRD and FTIR, all characterisation was carried out on powder samples stored for at least 24 h at 50% relative humidity, to allow for equal hydration states.

Powder X-ray diffraction (XRD) was undertaken with a Bruker D8 Advance instrument using monochromatic CuKα1 L3 (λ = 1.540598 Å) X-radiation and a Vantec superspeed detector. A step size of 0.016 °(2θ) and step duration of 0.3 s

were used. Oriented powder samples were used, prepared using a glass slide to press down the powder onto another glass slide. This preparation was chosen in order to achieve preferential orientation of clay minerals along their basal plane, and thus make them easier to identify when present in small quantities (Brindley and Brown, 1980). Phase identification was performed using Bruker EVA software. Patterns were corrected for sample height shift by calibrating to the most intense quartz reflection (101) at 26.6 °(2θ), and normalised to the most intense peak in each pattern.

For each of the activated clay mixtures, a Rule of Mixtures (RoM) XRD pattern was calculated and plotted, to compare with the measured pattern for each activated sample. The RoM XRD patterns were calculated by proportionally summing the raw data of the XRD patterns for the constituent activated clays. For example, the calculated RoM pattern for activated 50Kao-50Mont was generated by summing together the activated Kao pattern at 50% intensity, and the activated Mont pattern at 50% intensity. The calculated pattern was then normalised in the same way as for the measured patterns. As XRD intensity is affected by particle orientation and other factors, this is not considered an exact prediction but was used to make a very rough comparison between each clay mixture's measured pattern, and what would be expected from a RoM model. This method gave good agreement to the measured pattern when comparing the control mixtures of clays. Due to the limitations of the XRD preparation techniques used, it was not possible to make quantitative comparisons. However, for the purpose of identifying differences in phases formed and any large differences in the quantities of phases formed, this method was deemed acceptable.

Scanning electron microscope (SEM) imaging was used to characterise phase size and morphology, using a JEOL SEM6480LV in secondary electron mode with an accelerating voltage (AV) of 10 kV. Bulk specimens were sputter coated with gold for 3 min. All images were taken >2 mm away from the edge to minimise edge effects.

Fourier Transform Infrared Spectroscopy (FTIR) was performed to characterise molecular bonding, using a Perkin-Elmer Frontier with a diamond Attenuated Total Reflectance (ATR) head. Spectra were collected over a range of 4000-600 cm^{-1} using a resolution of 4 cm^{-1} and 5 scans per spectrum. Corrections were made for

ATR and background using Perkin-Elmer Spectrum software, and each spectrum was normalised relative to its most intense band. RoM spectra were calculated for the clay mixtures using the same method described for the RoM XRD patterns.

3 Results

3.1 Visual inspection

A range of colour and form was observed in the cured samples (Figure 2). The influence of ≥50% montmorillonite was strong, giving distinctive angled shrinkage cracking. The reasons for the distinctive form of these shrinkage cracks are not yet known, but these were consistent with similar cracks previously observed in alkali activation of this montmorillonite clay (Marsh et al., 2018a). There was a clear band of darker colour at the top of the 33Kao-33Mont-33ILL sample, and to a lesser extent, some darkening at the top of the 50ILL-50Kao sample. These phenomena are likely to be associated with the one-dimensional flow of soluble matter to the top of the sample, given that a mould with one open end was used.

Figure 2: Photos of the cured activated mixed clay samples.

3.2 XRD

In the figures for XRD, for purposes of clarity given the number of patterns shown, only the main reflections for the clay minerals and reflections for product phases are indexed. In general, most of the reflections above 40 °2θ correspond to unreactive phases. Full indexation of reflections in the precursors' patterns is given in Figure 1.

3.2.1 Kao-Mont series

Firstly considering the individual clays at each end of this series, alkali activation of kaolinite and montmorillonite under these conditions has already been shown to form a 8:2:2 hydrosodalite (Marsh et al., 2018b) – a member of the sodalite and zeolite families - and a N-A-S-H geopolymer (Marsh et al., 2018a) respectively. 90Kao-10Mont formed the same hydrosodalite phase and a small amount of hydroxycancrinite (Figure 3). 50Kao-50Mont formed a trace amount of hydrosodalite and a small amount of thermonatrite ($Na_2CO_3 \cdot H_2O$). 10Kao-90Mont formed a small amount of thermonatrite as the only crystalline product phase, but experienced a background shift in the 20 – 35 °2θ region (Figure 3b) indicative of geopolymer formation (Duxson et al., 2007a), whilst retaining a large amount of unreacted montmorillonite.

Amongst the activated samples, kaolinite was still present in all mixes originally containing kaolinite. Montmorillonite was still present in mixtures with ≥ 50% montmorillonite in the starting mix. It was not detectable in 90Kao-10Mont, but was only faintly detectable in the control sample. The montmorillonite 001 reflection consistently shifted from 5.9 to 7.3 °2θ after activation, corresponding to a decrease of d-value from 14.4 to 11.6 Å. For this particular montmorillonite clay, this phenomenon is due to a combination of interlayer cation exchange for the Na in solution, as well as other possible effects associated with alkali activation (Marsh et al., 2018a). Muscovite was present in all samples, with no significant change in °2θ position, as expected from previous work by Zografou (2015).

In summary, hydrosodalite formed in mixtures with ≥90% kaolinite, but not for samples with <50% kaolinite. Hydroxycancrinite formed in 90Kao-10Mont, but in no others. A geopolymer hump seemed to form in samples with ≥50% montmorillonite, but was a more subtle change for 50Kao-50Mont (Figure 3b).

The RoM patterns were broadly correct in predicting the product phases formed, but were not consistent over the whole series. For 90Kao-10Mont the RoM model predicted hydrosodalite as a major product phase, while in the measured pattern, a small amount of hydroxycancrinite was formed in addition to hydrosodalite. For 50Kao-50Mont, hydrosodalite was predicted as a major phase, whereas only a trace amount was formed. For 90Mont-10Kao, it was correctly predicted that a large

amount of montmorillonite remained unreacted, but the prediction that a minor amount of hydrosodalite would form could not be confirmed from the XRD pattern.

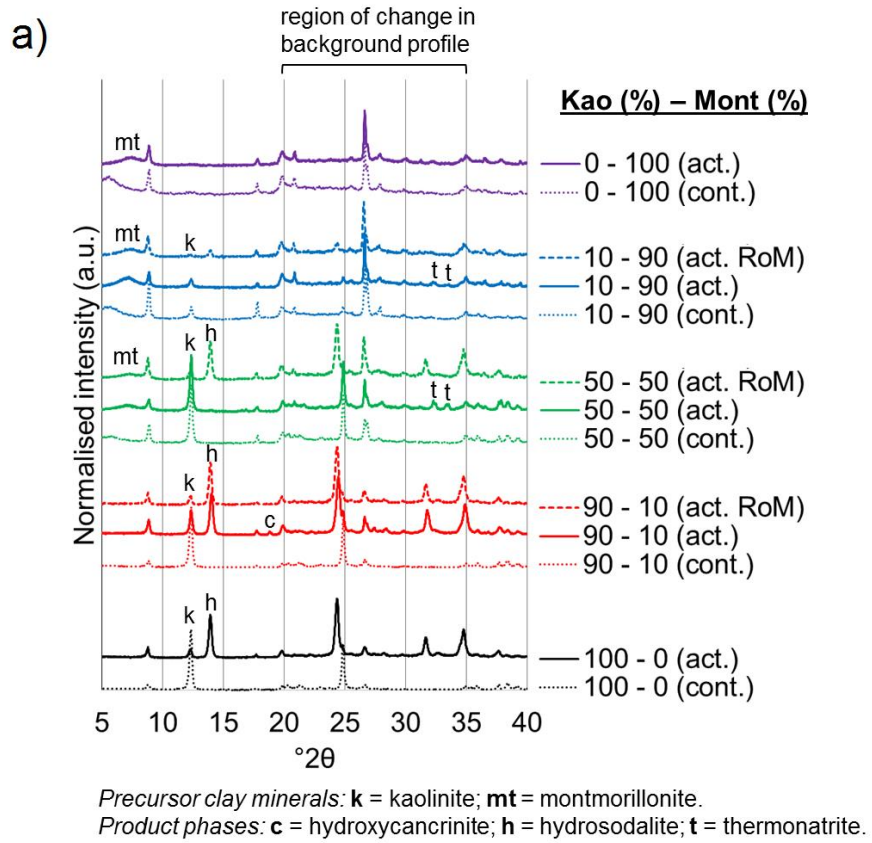

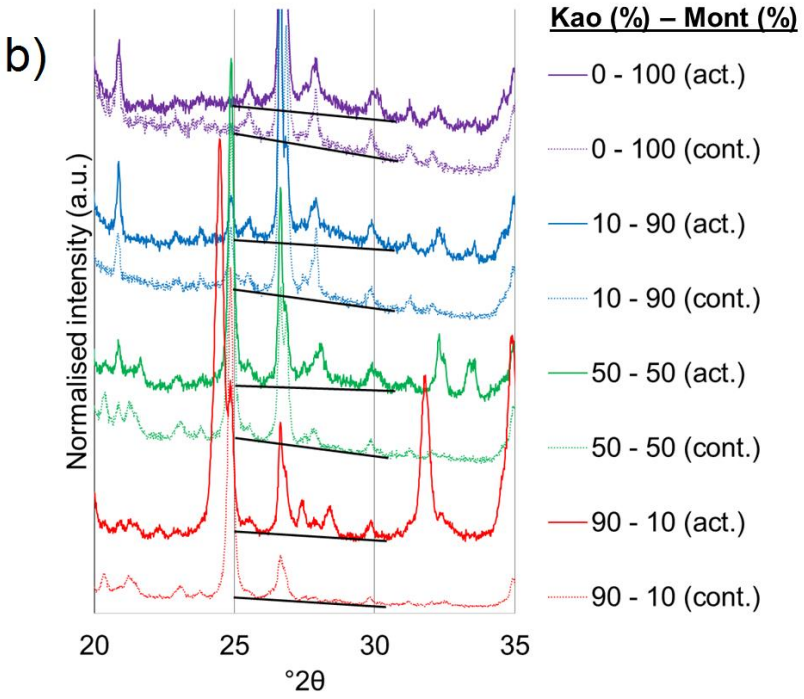

Figure 3: Kao-Mont series: a) XRD patterns of control (cont.) samples, compared with measured (act.) and RoM calculated (act. RoM) patterns of the activated samples. b) XRD patterns for a selection of samples for the range 20 – 35 °2θ. Lines have been drawn to illustrate the changes in the backgrounds of the patterns from 25 – 30 °2θ.

3.2.2 Mont-ILL series

Firstly considering the individual clays at each end of this series, alkali activation of montmorillonite under these conditions has already been shown to form a N-A-S-H geopolymer (Marsh et al., 2018a). For the alkali activation of illite under these conditions, the outcome is to alter the microstructure of illite, but without any clear changes in the crystal structure – a full description is given in the study by Marsh et al. (2018a). 50Mont-50ILL formed a small amount of thermonatrite ($Na_2CO_3 \cdot H_2O$) as the only new crystalline phase (Figure 4). Montmorillonite shifted its 001 reflection position as already observed in the previous series. The trace kaolinite impurity, evident by the reflection at 12.5 °2θ in the control sample's pattern, appeared to be consumed. However, there was no evidence for formation of a hydrosodalite reflection, as observed for consumption of trace kaolinite in 0Mont-100ILL. The illite reflections at 9 and 18 °2θ overlapped with those of the muscovite impurity in the montmorillonite precursor. These reflections appeared to decrease in intensity, but the reflections at 20 °2θ were maintained, which could suggest this was partly an orientation effect. In each measured pattern, a large amount of clay precursor was still present, as shown in the 5 - 10 °2θ region.

The RoM model matched well with the measured pattern. The only difference was the prediction of a trace amount of hydrosodalite, which was not observed in the measured pattern of 50Mont-50ILL. Given that both the reaction products from individual activated montmorillonite and illite do not appear as new crystalline reflections, the good match between the RoM model and the measured pattern was not in itself conclusive. However, the background profiles of the measured and RoM patterns were broadly similar.

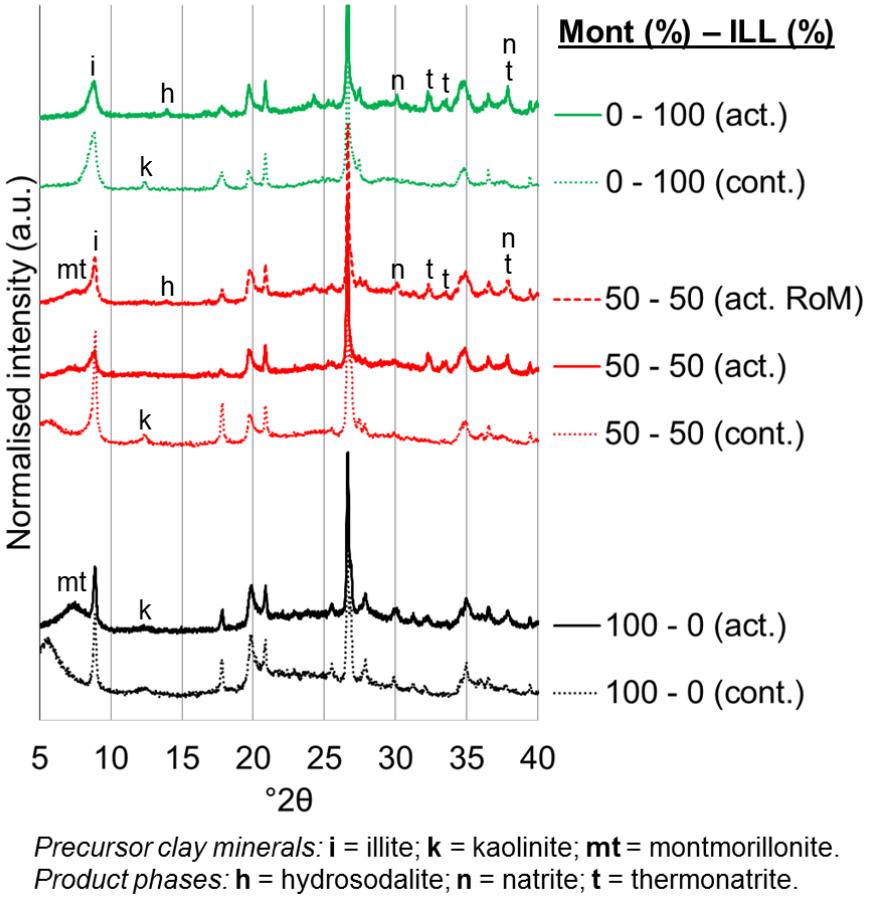

Figure 4: Mont-ILL series: XRD patterns of control (cont.) samples, compared with measured (act.) and RoM calculated (act. RoM) patterns of the activated samples.

3.2.3 ILL-Kao series

Firstly considering the individual clays at each end of this series, alkali activation of illite and kaolinite under these conditions has already been shown to form altered illite (Marsh et al., 2018a) and 8:2:2 hydrosodalite (Marsh et al., 2018b) respectively. In 50ILL-50Kao, hydrosodalite was the major crystalline reaction product with possibly a trace amount of hydroxycancrinite, although some reflections overlapped with those of microcline and thermonatrite (Figure 5). All the kaolinite in the precursor seemed to be consumed, but unreacted illite was still present. However, as previously stated, the 001 reflection overlapped with that of the muscovite, which undergoes very limited dissolution in alkali solutions.

The RoM pattern correctly predicted that hydrosodalite was the dominant product phase for 50ILL-50Kao sample. However, it predicted a minor amount of kaolinite phase would remain in the 50% mixture, whilst the measured pattern showed only a trace amount.

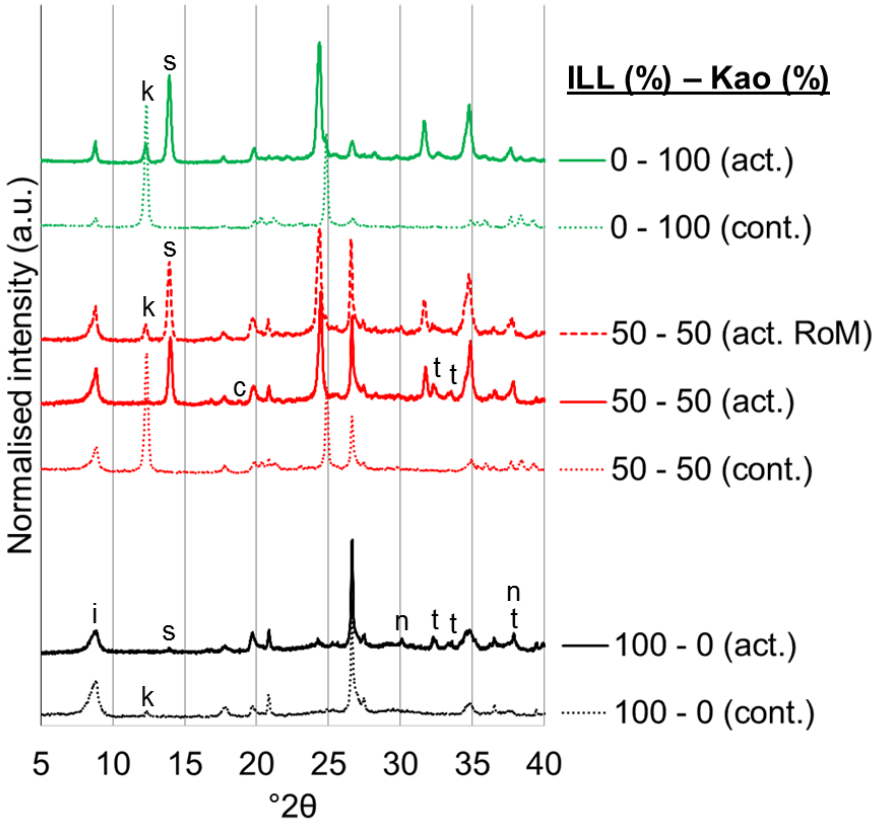

Figure 5: ILL-Kao series: XRD patterns of control (cont.) samples, compared with measured (act.) and RoM calculated (act. RoM) patterns of the activated samples.

3.2.4 Kao-Mont-ILL

In the mix of all three clay precursors, hydrosodalite was formed as the major crystalline product phase (Figure 6). There was some evidence of a shift in background profile towards higher angles in the 20 - 35 °2θ region. Some kaolinite and montmorillonite was consumed, with some left as a remnant. The overlap of the first two illite reflections with those of muscovite made it difficult to discern whether the intensity of these had decreased after activation. The RoM model was correct in predicting hydrosodalite as the main reaction product, as well as a small change in the background profile in the 20 – 25 °2θ region.

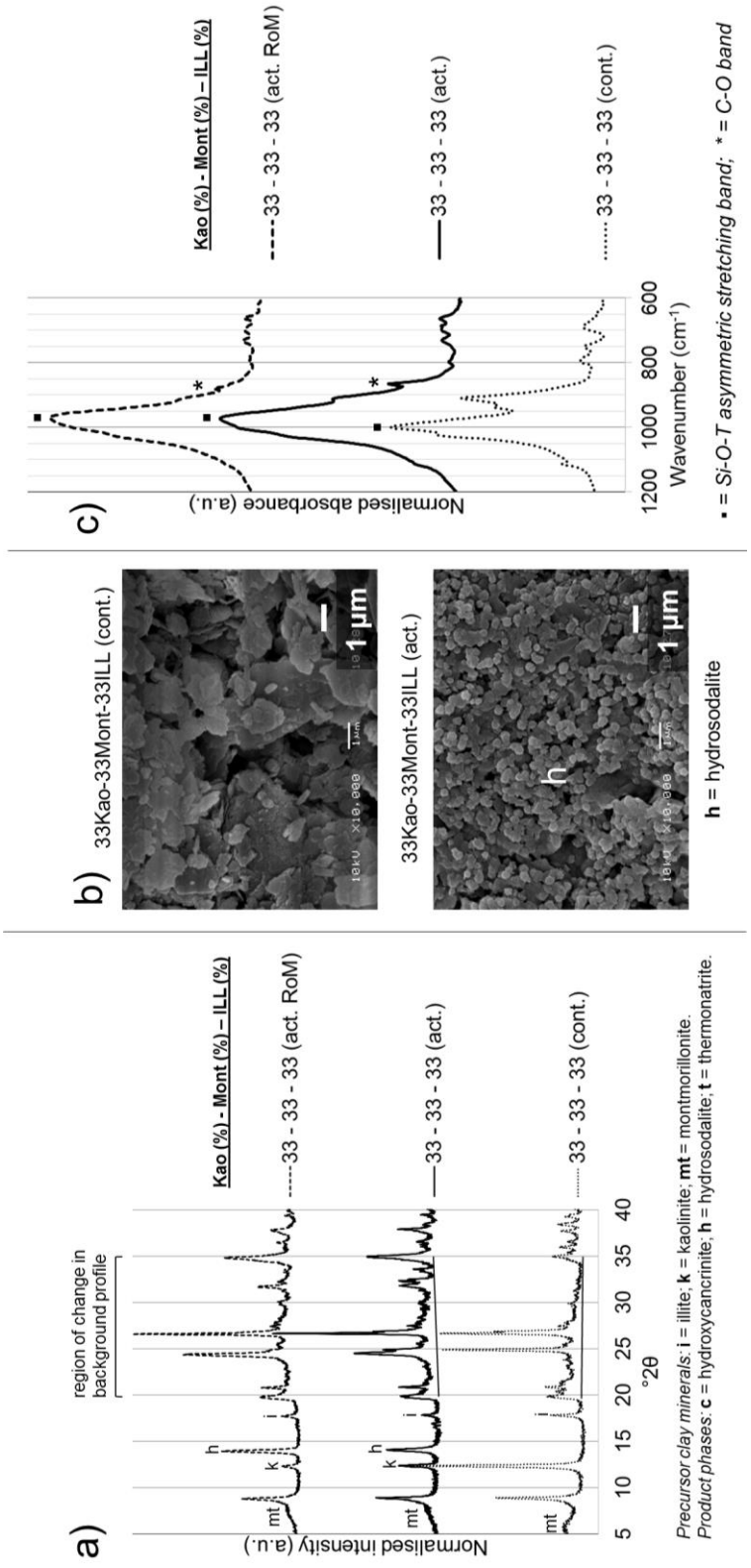

Figure 6: Combined results for the Kao-Mont-ILL series: a) XRD pattern of the control (cont.) sample, compared with measured (act.) and RoM calculated (act. RoM) patterns of the activated sample. Lines have been drawn to illustrate the changes in the backgrounds of the patterns from 20 – 35 °2θ. b) SEM images, comparing the cont. and act. samples. c) FTIR spectrum of the cont. sample, compared with act. and act. RoM spectra of the activated sample.

3.3 SEM

3.3.1 Kao-Mont series

Small, spheroidal crystallites were observed for 100Kao-0Mont and 90Kao-10Mont, typically with size of 250-500 nm and an irregular morphology (Figure 7). It was known from the XRD results that a large amount of hydrosodalite had formed in both of these samples. Given that these spheroidal particles had a morphology similar to that expected from hydrosodalites (Moloy et al., 2016), they were attributed as hydrosodalite. The amount of hydrosodalite formed was less for 50Kao-50Mont than for the samples with >50% kaolinite, with a corresponding increase in unreacted kaolinite. For 10Kao-90Mont, there was a large quantity of new particles with irregular morphology and particle size of around 250 nm, with more of a connected structure between particles. At 0% kaolinite (100% montmorillonite), the new particles were semi-continuous. Both of these microstructural characteristics have previously been observed in geopolymer systems (Duxson et al., 2005). Given that no hydrosodalite or other crystalline phase was present in the XRD pattern for the 10% kaolinite sample, it was inferred that the new particles observed in both 10Kao-90Mont and 0Kao-100Mont samples were part of a N-A-S-H geopolymer phase.

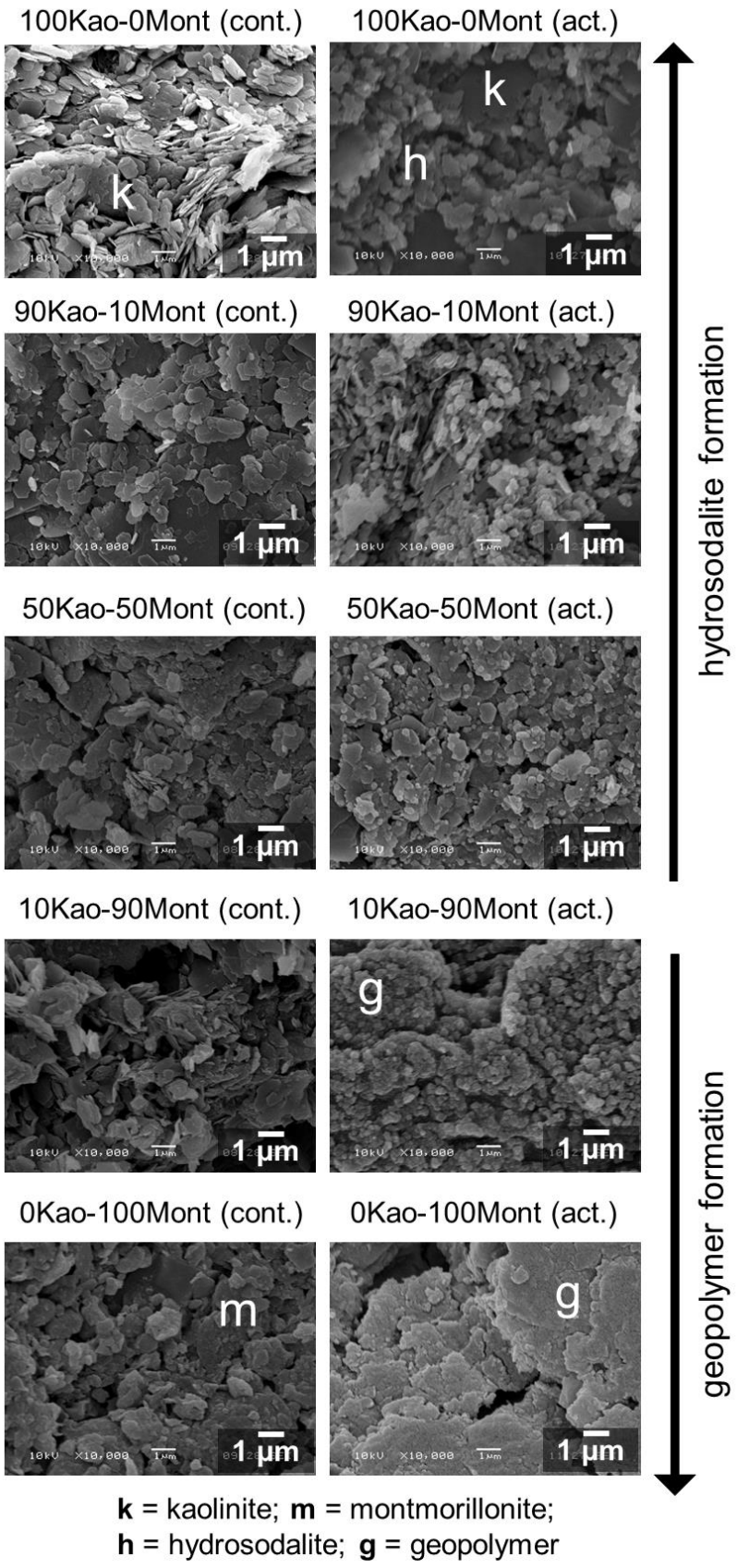

Figure 7: Kao-Mont series: SEM images comparing the control (cont.) and activated (act.) samples for each mixture.

3.3.2 Mont-ILL series

In 50Mont-50ILL, the microstructure was made of irregular particles of 100-500 nm, sometimes showing connectedness (Figure 8).This is different to the microstructures of both 100Mont-0ILL, a semi-continuous geopolymer, and 0Mont-100ILL, an altered illite with a distinctive arrangement of particles (Marsh et al., 2018a). Given that the XRD pattern revealed no crystalline product phase, and that geopolymers have been observed to have similar particle morphologies (Duxson et al., 2005), this new microstructure was also attributed to be a N-A-S-H geopolymer. This was similar to the microstructure of the 10Kao-90Mont sample, also attributed to be a N-A-S-H geopolymer for the same reasons.

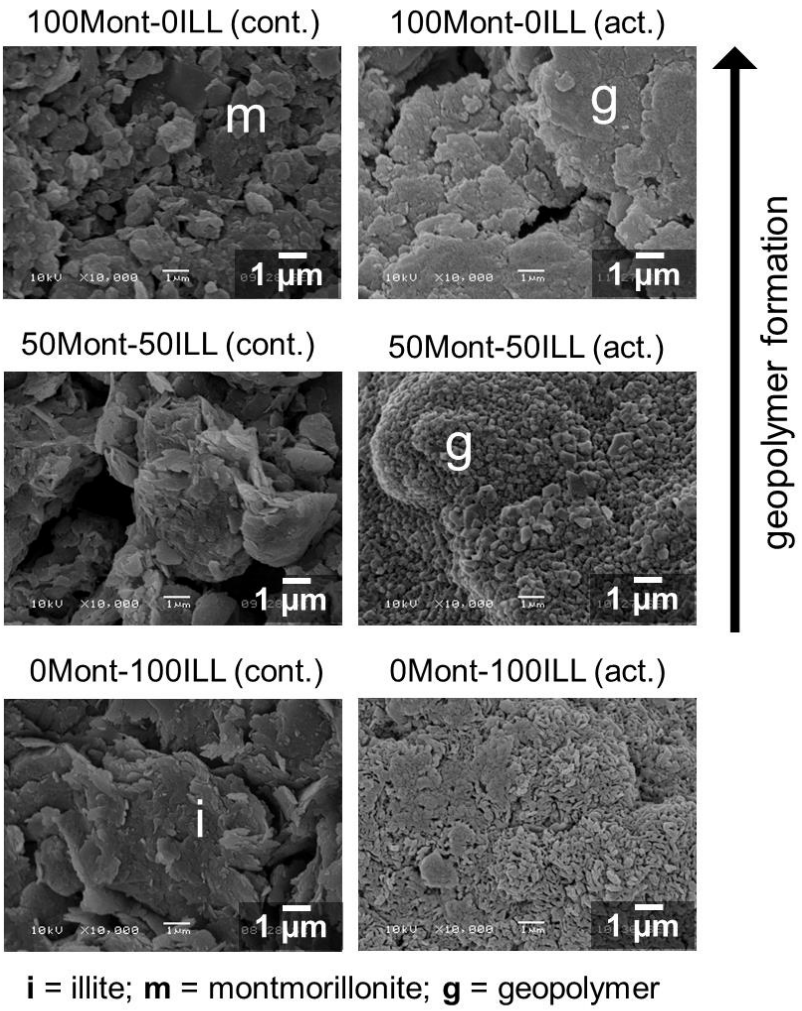

Figure 8: Mont-ILL series: SEM images comparing the control (cont.) and activated (act.) samples for each mixture.

3.3.3 ILL-Kao series

In 50ILL-50Kao, the microstructure was made of irregular particles of size 250-500 nm (Figure 9). Given that the control sample contained clay particles of similar dimensions, the change in appearance after activation was not dramatic. Some unreacted clay particles were still present in the activated sample. The XRD pattern for 50ILL-50Kao showed that a large amount of hydrosodalite was present, and the particles' morphology was in line with that expected of hydrosodalite (Moloy et al., 2006). From this evidence, the irregular particles seen in the SEM images were identified as hydrosodalite. The modified microstructure seen in 100ILL-0Kao was not observed in 50ILL-50Kao.

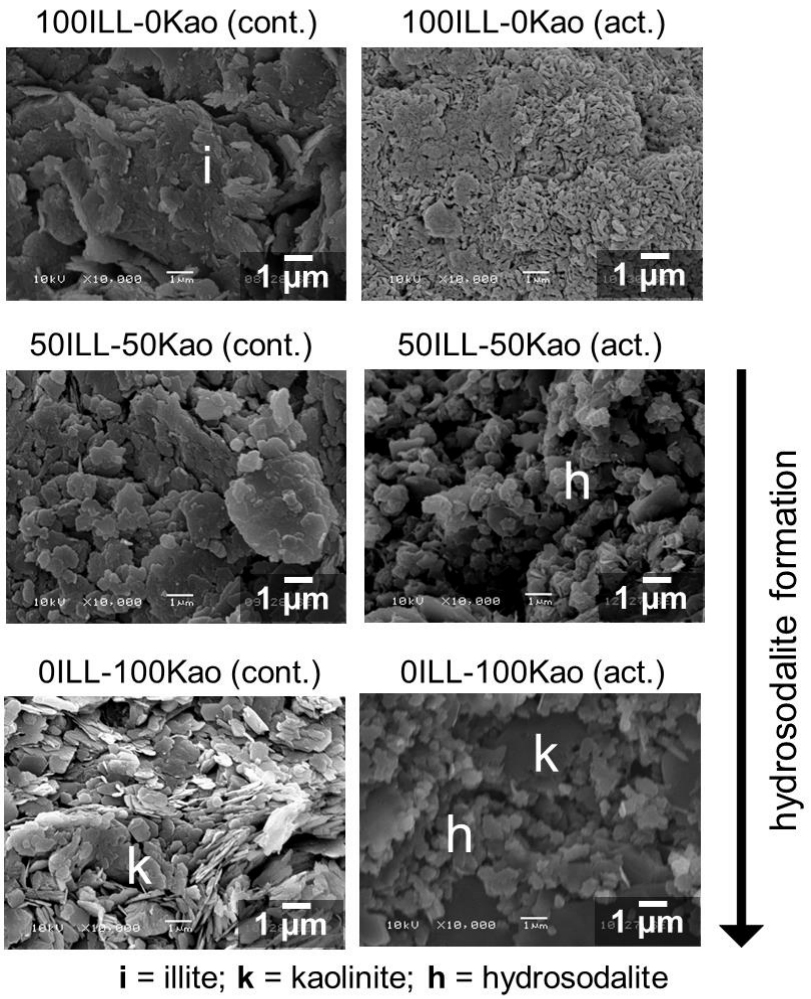

Figure 9: ILL-Kao series: SEM images comparing the control (cont.) and activated (act.) samples for each mixture.

3.3.4 Kao-Mont-ILL

The 33Kao-33Mont-33ILL sample contained a microstructure made of fine particles of size ~300 nm (Figure 6). Unreacted clay particles were present too. The XRD pattern for this sample showed hydrosodalite to be the crystalline reaction product, and the fine particles observed had a morphology in line with that expected of hydrosodalite (Moloy et al., 2006), so these were attributed as hydrosodalite.

3.4 FTIR

The most intense bands in the FTIR spectra were observed between 950 – 1080 cm^{-1}. This region is dominated by the Si-O-T (T = tetrahedral Si or Al) bands of the clay mineral precursor phases and alkali aluminosilicate product phases respectively.

The dominant band in each of the precursor clay minerals is the Si-O-T stretching vibration in the 970 - 1070 cm^{-1} region (Farmer, 1974; Madejova and Komadel, 2001). Si-O-T has been used here for the clay minerals rather than Si-O-Si, as other arrangements such as Si-O-Al can also be present. The dominant band in both of the crystalline alkali aluminosilicate product phases, hydrosodalite and hydroxycancrinite, is an asymmetric Si-O-Al stretching vibration in the region of 980 - 1000 cm^{-1} (Flanigen et al., 1974; Henderson and Taylor, 1977; Mikuła et al., 2015). In a geopolymer, it is an Si-O-T asymmetric stretching vibration (Rees et al., 2007b), the position of which depends on the Si:Al composition of the gel (Roy, 1990), the number of non-bridging oxygens and the extent of activation (Fernández-Jiménez and Palomo, 2005; Lee and van Deventer, 2003; Rees et al., 2007a).

Outside of this main region of interest, quartz has bands at Si-O stretching vibrations at around 778 and 798 cm^{-1} (Van der Marel and Beutelspacher, 1976). In the cured samples' spectra, carbonate bands are often seen in alkali-activated systems, with a C-O band at around 880 cm^{-1} (Barbosa et al., 2000).

3.4.1 Kao-Mont series

There were two clear groupings amongst the activated samples' FTIR spectra in this series (Figure 10). The main Si-O-T band region of 1200 - 800 cm^{-1} was similar between 100Kao-0Mont and 90Kao-10Mont, with a single band with a centre at ~965 cm^{-1}, indicating hydrosodalite formation. For the three other spectra for samples with ≥50% Mont, the main band area was broader with the band centres at higher

wavenumbers in the region of 995 - 1005 cm^{-1} indicating geopolymer formation. In this latter group, a carbonate band emerged at ~870 cm^{-1}.

Behaviour in the lower wavenumber region supported this interpretation. For 100Kao-0Mont and 90Kao-10Mont, bands emerged at ~663 and ~732 cm^{-1} attributed to hydrosodalite Si-O-Al symmetric stretching modes (Henderson and Taylor, 1977). In the other three spectra, no narrow new bands were formed in this region. This discounted the possibility of formation of nanocrystalline zeolitic phases in large amounts, with the emergence of a weak broad hump in this region suggesting geopolymer formation instead (Rees et al., 2007a).

The RoM spectra for activated 90Kao-10Mont and 10Kao-90Mont matched well with the measured spectra. However, for activated 50Kao-50Mont, there were clear differences in the RoM and measured spectra. The RoM spectrum's profile was broader, and the Si-O-T main band peak was at a lower wavenumber (968 cm^{-1}) than for the measured spectrum (1004 cm^{-1}). Given the association between a negative shift of the main Si-O-T band and formation of alkali aluminosilicate product phases (Prud'homme et al., 2013), the difference in Si-O-T band wavenumber suggests that a smaller extent of transformation occurred in the 50Kao-50Mont mixture than was expected from the behaviour of the individual clays.

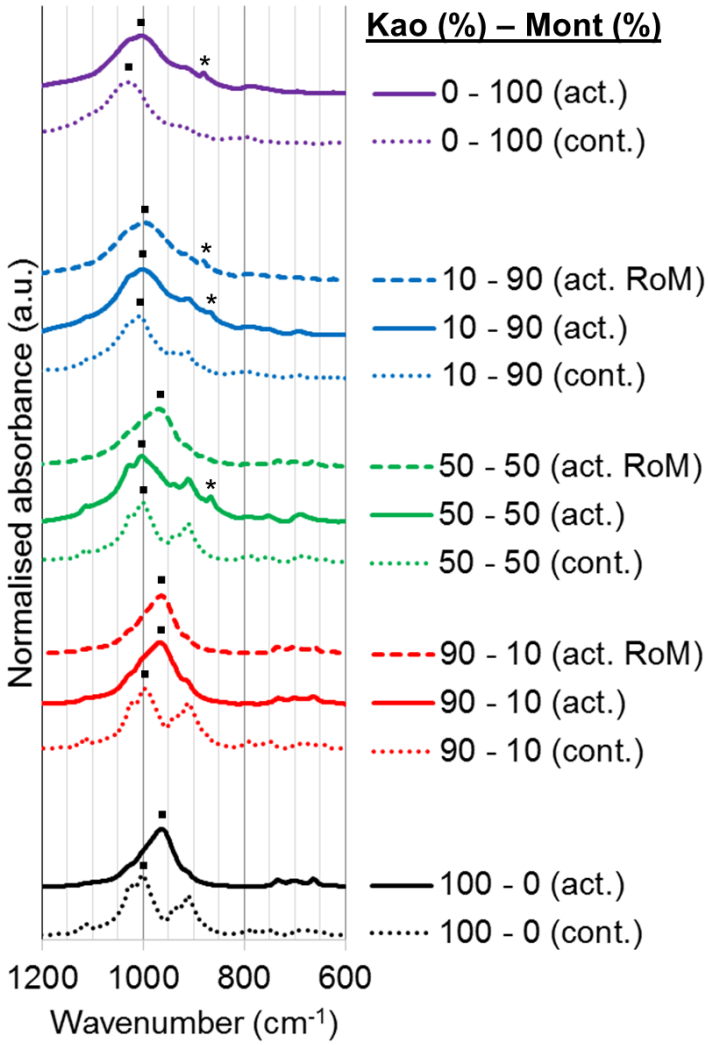

Figure 10: Kao-Mont series: FTIR spectra of the control (cont.) samples, compared with measured (act.) and RoM calculated (act. RoM) spectra of the activated samples.

3.4.2 Mont-ILL series

The end members of this series behaved differently after activation (Figure 11). The dominant band in 100Mont-0ILL shifted from 1031 cm^{-1} to a lower wavenumber at 1003 cm^{-1} after activation, indicating geopolymer formation, whereas the dominant band in 0Mont-100ILL shifted from 987 cm^{-1} to a slightly higher wavenumber at 994 cm^{-1}. For 50Mont-50ILL, the dominant band shifted from 1004 cm^{-1} to a slightly lower wavenumber at 992 cm^{-1} after activation and no narrow zeolitic bands emerged in the 650 - 750 cm^{-1} region. Given the microstructural changes observed in the SEM images, this also supported the interpretation that a geopolymer was formed in 50Mont-50ILL. A carbonate band emerged at 866 cm^{-1}. The RoM spectrum for activated 50Mont-50ILL matched well with the measured spectrum.

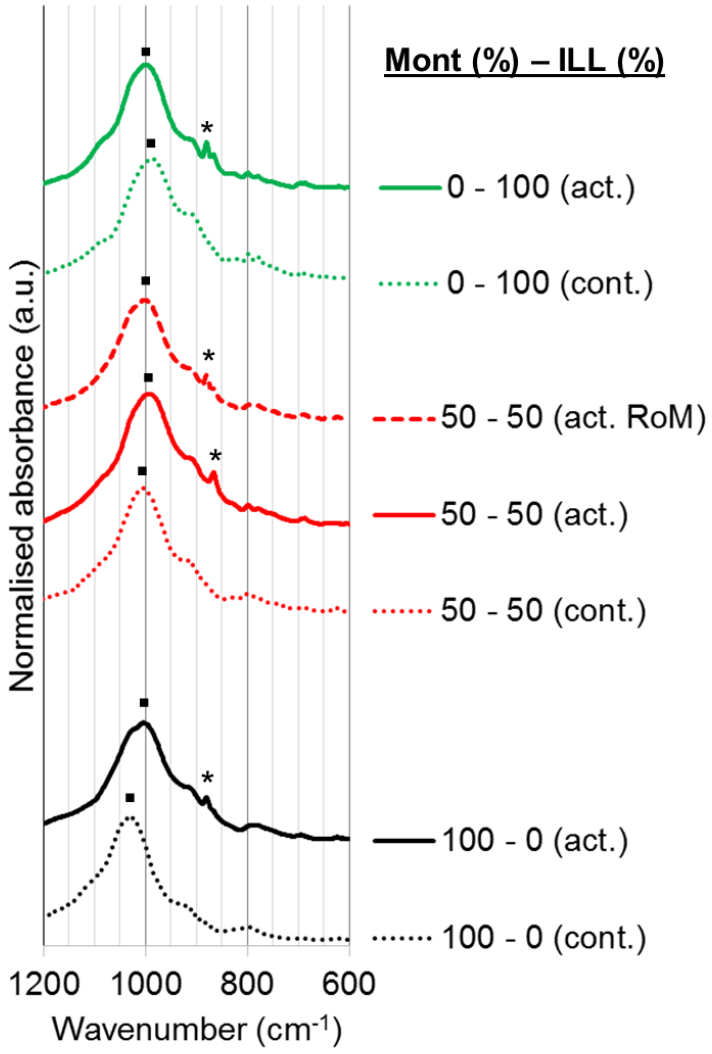

▪ = *Si-O-T asymmetric stretching band;* * = *C-O band*

Figure 11: Mont-ILL series: FTIR spectra of the control (cont.) samples, compared with measured (act.) and RoM calculated (act. RoM) spectra of the activated samples.

3.4.3 ILL-Kao series

In the spectrum of the activated 50ILL-50Kao sample, the dominant band moved to a lower wavenumber at 968 cm^{-1} and Si-O-T symmetric stretching bands emerged at 664 and 735 cm^{-1} (Figure 12).These observations supported the evidence of the XRD pattern that a hydrosodalite is the dominant reaction product. A carbonate band emerged at 866 cm^{-1}. The RoM spectrum for activated 50ILL-50Kao matched well with the measured spectrum.

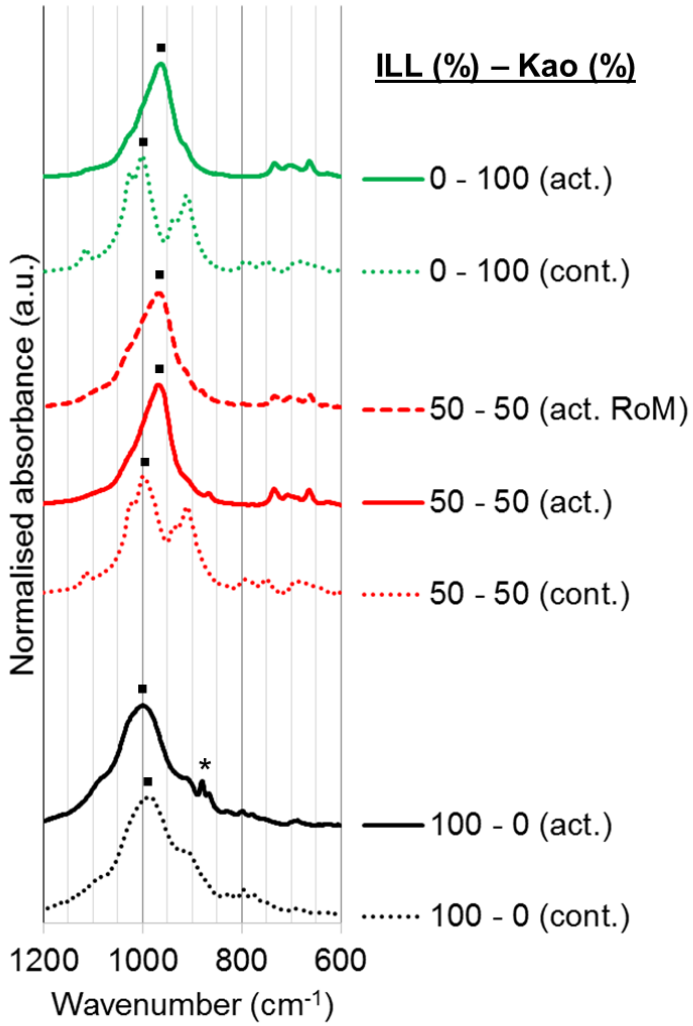

Figure 12: ILL-Kao series: FTIR spectra of the control (cont.) samples, compared with measured (act.) and RoM calculated (act. RoM) spectra of the activated samples.

3.4.4 Kao-Mont-ILL

After activation, the dominant band centre in the 33Kao-33Mont-33ILL spectrum shifted from 1000 cm^{-1} to 975 cm^{-1} and Si-O-T symmetric stretching bands emerged at 664 and 732 cm^{-1} (Figure 6). Hydrosodalite was known to be present from the XRD patterns, but given the presence of montmorillonite, a geopolymer phase may have also formed. The observed shift of the Si-O-T band centre may support this - the band centre was at a higher wavenumber than in activated samples which contained hydrosodalite as the primary reaction product (100Kao-0Mont and 50ILL-50Kao), but lower than in activated samples which contained a geopolymer as the primary reaction product (0Kao-100Mont and 10Kao-90Mont). An intermediate value of wavenumber for the Si-O-T band could therefore indicate the presence of a geopolymer phase as well as hydrosodalite. As with other samples, a carbonate band emerged at 866 cm^{-1}. The RoM spectrum for activated 33Kao-33Mont-33ILL matched well with the measured spectrum.

For all the clays and clay mixtures except illite and 50Kao-50Mont, there was a decrease in wavenumber of the main Si-O-T band after activation.

3.4.5 Changes in wavenumber position of dominant band

As previously used in studies investigating the variables of time (Essaidi et al., 2014), alkali source and calcination temperature (Prud'homme et al., 2013), the position of the dominant Si-O-T band in the sample can help understand product phases formed in alkali activation. As previously stated, the main region of interest is from approximately 950 – 1080 cm^{-1}, as this is dominated by the Si-O-T bands of the precursor and product phases. There was large variation in wavenumber of the dominant band between precursor samples, and between activated samples. There was also significant variation between samples in the change in Si-O-T band wavenumber after activation (Figure 13). In most, but not all cases, alkali activation resulted in a decrease in wavenumber position of the dominant band, as a result of more Si-O-Al bonds (relative to the number of Si-O-Si bonds) in the aluminosilicate framework (Fernández-Jiménez and Palomo, 2005). The extent of shift for geopolymer formation was less than the 40 cm^{-1} observed by Prud’homme et al. (2013), as might be expected since calcined clays were used in those experiments. However, for 50Kao-50Mont and 0Mont-100ILL / 100ILL-0Kao, there was a positive shift. No explanation of this positive shift has been yet found in the literature.

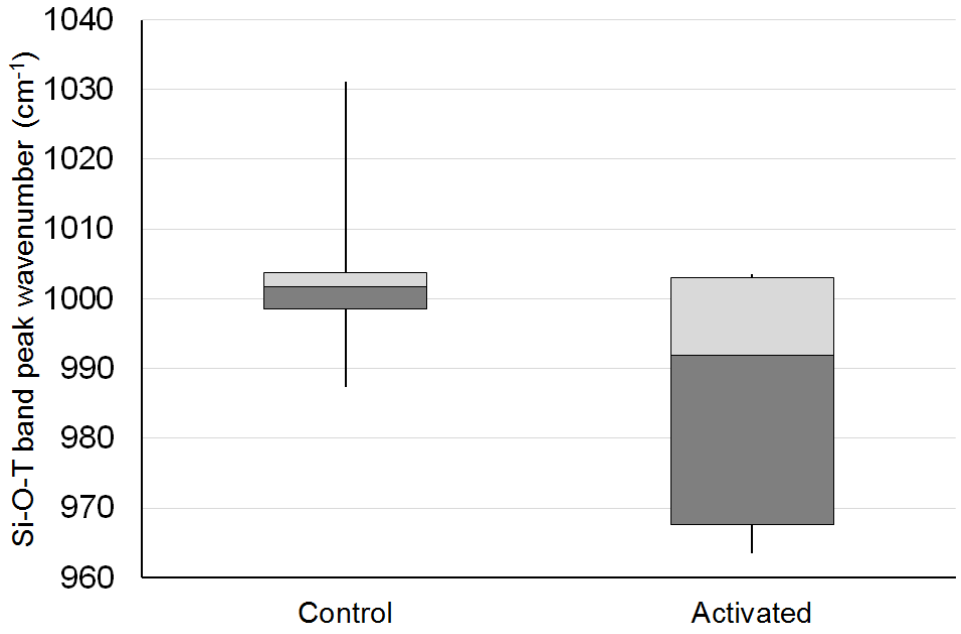

Figure 13: The distribution of wavenumbers for the Si-O-T band peak centre for control and activated samples. The centre-line of each box is the median value; the edges of each box are the first and third quartile values, and the lines extend to the maximum and minimum values.

4 Discussion

4.1 Evaluation of phase formation

Mixtures of clays are complex to characterise, even without alkali activation. Furthermore, given the amorphous nature of the geopolymer phase, it is important to use multiple characterisation methods to provide corroborating evidence. It has previously been shown that in the alkali activation of clays, different reaction products can coexist, including different zeolitic phases (Barrer and Mainwaring, 1972) and a zeolite with a geopolymer (Heller-Kallai and Lapides, 2007). Due to the multiple phases present, the amorphous character of geopolymers and the presence of some phases in small amounts, it is not possible to state the phase composition of the activated systems with complete certainty. Nonetheless, a summary of phases observed in the activated samples, as well as the phases predicted from the RoM model, is given in Table 3.

The trends observed here suggest that the wavenumber of the Si-O-T FTIR band could be a useful indicator for the alkali aluminosilicate phase formed in a given system of uncalcined clay mixtures, as has previously been shown for fly ash (Fernández-Jiménez and Palomo, 2005) and calcined clays (Prud'homme et al.,

2013). However, given the inconsistencies within the series here, it should not be relied on as a standalone method, but should be supported with complementary characterisation techniques. This is especially important for uncalcined clay mixtures. Given the coexistence of crystalline and amorphous phases, as well as the significant amount of unreacted precursors, phase identification is more complex and less certain than for simpler, more reactive systems such as metakaolin.

Regarding carbonate phase formation (not included in Table 3 for concision), a C-O band was detected in all of the samples where carbonates had been identified from the XRD pattern. In 0Kao-100Mont, a C-O band was detected, but no carbonate phase was identified in the XRD pattern. These two observations suggest two further insights. Firstly, that in most - if not all - of these systems there is an excess of Na available, which carbonates when not consumed during the reaction. And secondly, that the presence of carbonates in these systems cannot reliably be detected solely using XRD.

Table 3: A summary of the product phases observed through characterisation for the activated clay mixtures, and the product phases expected from the rule of mixtures model. Phases marked with a ? indicate less certainty.

Series	Sample	Phases observed	Phases expected from RoM model
Kao-Mont	90Kao-10Mont	Hydrosodalite Hydroxycancrinite	Hydrosodalite Geopolymer
	50Kao-50Mont	Hydrosodalite Geopolymer?	Hydrosodalite Geopolymer
	10Kao-90Mont	Geopolymer	Geopolymer Hydrosodalite
Mont-ILL	50Mont-50ILL	Geopolymer	Geopolymer Altered illite
ILL-Kao	50ILL-50Kao	Hydrosodalite Hydroxycancrinite?	Hydrosodalite Altered illite
Kao-Mont-ILL	33Kao-33Mont-33ILL	Hydrosodalite Geopolymer?	Hydrosodalite Geopolymer Altered illite

4.2 Performance of the rule of mixtures (RoM) model

For alkali-activated soils to be a viable construction technology, the phase formation behaviour needs to be predictable. As previously described, a rule of mixtures predictive model provides a useful basis for describing the phase formation behaviour of the clay mixtures.

For the Kao-Mont series in general, the RoM XRD patterns overpredicted the propensity of hydrosodalite formation. It predicted a large quantity of hydrosodalite for 50Kao-50Mont when only a trace amount was formed, and a minor quantity for 90Mont-10Kao when none was detected. It also did not predict the formation of a minor amount of hydroxycancrinite for 90Kao-10Mont. For the Mont-ILL series, the RoM pattern matched the measured pattern well, but since the expected transformations do not yield strongly crystalline signals, it is difficult to verify the accuracy of this. For the ILL-Kao series, the RoM model underestimated the extent of kaolinite consumption and hydrosodalite formation for 50ILL-50Kao.

The RoM FTIR spectra generally agreed well with the measured spectra, with the exception of 50Kao-50Mont. Here, the wavenumber of the Si-O-T band was higher in the measured pattern than in the RoM spectrum, suggesting that a smaller extent of transformation to alkali aluminosilicate reaction products occurred than expected. This agreed with the observation from the measured and RoM XRD patterns for 50Kao-50Mont, in that less hydrosodalite was formed than expected. Therefore, the evaluation of the FTIR RoM spectra is in broad agreement with the evaluation of the XRD RoM patterns.

Comparing the phases observed in the activated clay mixtures to those predicted by the RoM model, there is some degree of disagreement for nearly all of the mixtures. The RoM model is not consistently correct in predicting the phases and quantities formed in the alkali activation of mixtures of clays. This suggests there are hierarchies in the dissolution and subsequent reactivity of these clays and in determining the product phases formed. Given that consistent curing conditions were used for all compositions, the deviation from RoM behaviour is likely to be due to the conditions in the Al- and Si-rich pore solution favouring the production of different phases (Buchwald et al., 2011), and possibly the influence of the precursor minerals.

4.3 Dominance relations between clays in determining product phase formation

Given that the behaviour of the clay mixtures deviated from a rule of mixtures model, this can be used as a baseline to consider the dominance relations between the clays under the activation conditions used in this study. Dominance relations are evaluated here in two areas of interest – precursor reactivity, and product phase

formation. For example, in an alkali-activated clay mixture of A and B, if more of clay mineral A reacts and less of clay mineral B reacts (compared to the baseline behaviour in the RoM model), then clay mineral A could be said to be dominant in terms of reactivity. In the same mixture, if more of the product phase associated with clay mineral B forms than the product phase associated with clay mineral A (again, compared to the RoM model), then clay mineral B could be said to be dominant in terms of determining product phase formation in the mixture. Predicting the suitability of aluminosilicate precursors for alkali activation is acknowledged to be difficult even for individual minerals (Xu and Van Deventer, 2000), let alone for mixtures of minerals. The approach used here is not a quantitative method of evaluation, but is helpful in developing an empirical understanding of how such mixtures behave in alkali activation. In the following section, the constituent clay minerals' reactivity and influence on phase formation in the different mixtures are evaluated in this way.

In the Kao-Mont series as a whole, less kaolinite was consumed than expected from the RoM model, and less hydrosodalite was formed than expected. From the behaviour of the 50Kao-50Mont sample, montmorillonite seemed to be more reactive than kaolinite, given how much of each was consumed in the reaction. On the other hand, the characterisation evidence suggested that more hydrosodalite (the product phase associated with kaolinite) had formed compared to N-A-S-H geopolymer (the product phase associated with montmorillonite). Thus, over the Kao-Mont series as a whole, montmorillonite was dominant in terms of reactivity, but kaolinite was dominant in determining phase formation.

In the Mont-ILL series, there was evidence of a N-A-S-H geopolymer (the product phase associated with montmorillonite) but not of altered illite (the product associated with illite) in 50Mont-50ILL. Given the overlap between the illite reflections and the muscovite impurity reflections in this XRD pattern, it was not possible to compare the relative extents of reaction of the montmorillonite and illite. So, for the Mont-ILL series, one can only say that montmorillonite dominated illite in determining phase formation.

In the ILL-Kao series, the RoM model underestimated both the extent of kaolinite consumption and the extent of hydrosodalite formation (the product phase associated with kaolinite) in 50ILL-50Kao. At the same time, no microstructural

features similar to those in 100ILL-0Kao were observed in the SEM images of 50ILL-50Kao. So, for the ILL-Kao series, kaolinite dominated illite both in reactivity and in determining product phase formation.

The validity of this interpretation can be checked against 33Kao-33Mont-33ILL, as this mixture includes the three constituent clay minerals together. As summarised in Table 3, the XRD pattern and SEM images showed hydrosodalite to be present, with no evidence of the microstructure characteristic of altered illite. There was possibly a background hump indicative of a geopolymer in the XRD pattern, with the position of the dominant Si-O-T band in the FTIR spectrum suggesting a possible mix of geopolymer and hydrosodalite. These observations broadly agree with the dominance relations established from the three binary series of clay mixtures.

These dominance relations have been evaluated for these specific clay precursors, under the alkali activation conditions used in this study. The chemistry and mineralogy of the clay minerals is highly influential in determining their reactivity and product phase formation. However, it is unlikely to be the case that these are inherent, irrevocable qualities of the clay minerals. It is conceivable that these dominance relations could change depending on other factors influencing dissolution, such as available surface area (Tchadjie and Ekolu, 2018), and phase formation, such as curing temperature, curing time and concentration of NaOH activating solution (Abdullahi et al., 2017; Johnson and Arshad, 2014).

Nonetheless, this finding has implications for the application of alkali-activated clays and soils in construction. The expansive behaviour of soils containing montmorillonite means they are typically avoided in earth construction. However, given that montmorillonite influences phase formation towards geopolymers, the presence of montmorillonite could be beneficial in alkali-activated soil materials, if enough of the montmorillonite can be consumed. Illite is much less expansive, so is normally considered acceptable in soil construction. In isolation, its alkaline activation behaviour is problematic, although could be useful when present as a minor component with other clay minerals. Although these dominance relations were established for un-calcined clays, and without using additional soluble silicates, it is an important step in improving the fundamental understanding of the behaviour of alkali-activated soils.

5 Conclusions

Through investigating the alkali activation of binary series of clay mixtures, it has been shown that there was a hierarchy between the clay minerals kaolinite, montmorillonite and illite in determining the product phases formed in the alkali activation of a clay mixture. Montmorillonite and kaolinite both dominated illite in terms of reactivity and determining phase formation. Montmorillonite seemed to be more reactive than kaolinite, but kaolinite had a stronger influence in determining reaction products. Hydroxycancrinite was formed in at least one of the binary mixtures, which was not a reaction product from any of the individual clays under these conditions. These findings suggest that knowing which clay minerals are present can help broadly predict phase formation; but, neither the relative amounts of phases formed, nor the type of phases formed, can be exactly predicted. The systematic method employed in this study has enabled a useful bridge to be made between the study of individual clays and complex soil systems.

Acknowledgements

This study was supported by the EPSRC Centre for Decarbonisation of the Built Environment (dCarb) [grant number EP/L016869/1] and a University of Bath Research Scholarship. All data created during this research are openly available from the University of Bath data archive at https://doi.org/10.15125/BATH-00563

References

Abdullahi, T., Harun, Z., Othman, M.H.D., 2017. A review on sustainable synthesis of zeolite from kaolinite resources via hydrothermal process. Advanced Powder Technology 28, 1827-1840.
Abe, S.S., Masunaga, T., Yamamoto, S., Honna, T., Wakatsuki, T., 2006. Comprehensive assessment of the clay mineralogical composition of lowland soils in West Africa. Soil Science & Plant Nutrition 52, 479-488.
Autef, A., Joussein, E., Gasgnier, G., Rossignol, S., 2012. Role of the silica source on the geopolymerization rate. Journal of Non-Crystalline Solids 358, 2886-2893.
Barbosa, V.F.F., MacKenzie, K.J.D., Thaumaturgo, C., 2000. Synthesis and characterisation of materials based on inorganic polymers of alumina and silica: sodium polysialate polymers. International Journal of Inorganic Materials 2, 309-317.
Barrer, R.M., Mainwaring, D.E., 1972. Chemistry of soil minerals. Part XIII. Reactions of metakaolinite with single and mixed bases. Journal of the Chemical Society, Dalton Transactions, 2534-2546.
Bauer, A., Berger, G., 1998. Kaolinite and smectite dissolution rate in high molar KOH solutions at 35° and 80°C. Applied Geochemistry 13, 905-916.
Belviso, C., Cavalcante, F., Niceforo, G., Lettino, A., 2017. Sodalite, faujasite and A-type zeolite from 2:1 dioctahedral and 2:1:1 trioctahedral clay minerals. A singular review of

synthesis methods through laboratory trials at a low incubation temperature. Powder Technology 320, 483-497.
Brindley, G.W., Brown, G., 1980. Crystal structures of clay minerals and their X-ray identification. Mineralogical Society, London.
Brunauer, S., Emmett, P.H., Teller, E., 1938. Adsorption of gases in multimolecular layers. Journal of the American chemical society 60, 309-319.
Buchwald, A., Zellmann, H.D., Kaps, C., 2011. Condensation of aluminosilicate gels—model system for geopolymer binders. Journal of Non-Crystalline Solids 357, 1376-1382.
Couchman, P.R., 1978. Compositional Variation of Glass-Transition Temperatures. 2. Application of the Thermodynamic Theory to Compatible Polymer Blends. Macromolecules 11, 1156-1161.
Criado, M., Fernández-Jiménez, A., Palomo, A., 2007. Alkali activation of fly ash: Effect of the SiO2/Na2O ratio: Part I: FTIR study. Microporous and Mesoporous Materials 106, 180-191.
Davidovits, J., 2011. Geopolymer chemistry and applications, 3rd ed. Institut Geopolymere, Saint-Quentin.
Diop, M.B., Grutzeck, M.W., 2008. Low temperature process to create brick. Construction and Building Materials 22, 1114-1121.
Dixon, J.B., Weed, S.B., 1989. Minerals in Soil Environments, 2nd ed. Soil Science Society of America, Madison, WI.
Donald, I.W., Davies, H.A., 1978. Prediction of glass-forming ability for metallic systems. Journal of Non-Crystalline Solids 30, 77-85.
Duxson, P., Fernández-Jiménez, A., Provis, J.L., Lukey, G.C., Palomo, A., van Deventer, J.S.J., 2007a. Geopolymer technology: the current state of the art. J Mater Sci 42, 2917-2933.
Duxson, P., Mallicoat, S.W., Lukey, G.C., Kriven, W.M., van Deventer, J.S.J., 2007b. The effect of alkali and Si/Al ratio on the development of mechanical properties of metakaolin-based geopolymers. Colloids and Surfaces A: Physicochemical and Engineering Aspects 292, 8-20.
Duxson, P., Provis, J.L., Lukey, G.C., Mallicoat, S.W., Kriven, W.M., van Deventer, J.S.J., 2005. Understanding the relationship between geopolymer composition, microstructure and mechanical properties. Colloids and Surfaces A: Physicochemical and Engineering Aspects 269, 47-58.
El Hafid, K., Hajjaji, M., 2015. Effects of the experimental factors on the microstructure and the properties of cured alkali-activated heated clay. Applied Clay Science 116–117, 202-210.
Essaidi, N., Samet, B., Baklouti, S., Rossignol, S., 2014. The role of hematite in aluminosilicate gels based on metakaolin. Ceramics Silikati 58, 1-11.
Farmer, V.C., 1974. Infrared spectra of minerals. Mineralogical society, London.
Fernández-Jiménez, A., Palomo, A., 2005. Mid-infrared spectroscopic studies of alkali-activated fly ash structure. Microporous and Mesoporous Materials 86, 207-214.
Ferrage, E., Lanson, B., Sakharov, B.A., Drits, V.A., 2005. Investigation of smectite hydration properties by modeling experimental X-ray diffraction patterns: Part I. Montmorillonite hydration properties. Am Mineral 90, 1358-1374.
Flanigen, E.M., Khatami, H., Szymanski, H.A., 1974. Infrared Structural Studies of Zeolite Frameworks, Molecular Sieve Zeolites-I. AMERICAN CHEMICAL SOCIETY, pp. 201-229.
Gailhanou, H., van Miltenburg, J.C., Rogez, J., Olives, J., Amouric, M., Gaucher, E.C., Blanc, P., 2007. Thermodynamic properties of anhydrous smectite MX-80, illite IMt-2 and mixed-layer illite–smectite ISCz-1 as determined by calorimetric methods. Part I: Heat capacities, heat contents and entropies. Geochimica et Cosmochimica Acta 71, 5463-5473.
Haines, S.H., van der Pluijm, B.A., 2008. Clay quantification and Ar–Ar dating of synthetic and natural gouge: Application to the Miocene Sierra Mazatán detachment fault, Sonora, Mexico. Journal of Structural Geology 30, 525-538.
Heller-Kallai, L., Lapides, I., 2007. Reactions of kaolinites and metakaolinites with NaOH—comparison of different samples (Part 1). Applied Clay Science 35, 99-107.

Henderson, C., Taylor, D., 1977. Infrared spectra of anhydrous members of the sodalite family. Spectrochimica Acta Part A: Molecular Spectroscopy 33, 283-290.
Hollanders, S., Adriaens, R., Skibsted, J., Cizer, Ö., Elsen, J., 2016. Pozzolanic reactivity of pure calcined clays. Applied Clay Science 132-133, 552-560.
Johnson, E.B.G., Arshad, S.E., 2014. Hydrothermally synthesized zeolites based on kaolinite: A review. Applied Clay Science 97-98, 215-221.
Lee, W.K.W., van Deventer, J.S.J., 2003. Use of Infrared Spectroscopy to Study Geopolymerization of Heterogeneous Amorphous Aluminosilicates. Langmuir 19, 8726-8734.
Lemougna, P.N., Madi, A.B., Kamseu, E., Melo, U.C., Delplancke, M.P., Rahier, H., 2014. Influence of the processing temperature on the compressive strength of Na activated lateritic soil for building applications. Construction and Building Materials 65, 60-66.
Liew, Y.M., Heah, C.Y., Mohd Mustafa, A.B., Kamarudin, H., 2016. Structure and properties of clay-based geopolymer cements: A review. Progress in Materials Science 83, 595-629.
Llatas, C., 2011. A model for quantifying construction waste in projects according to the European waste list. Waste Management 31, 1261-1276.
MacKenzie, K.J.D., 2009. Utilisation of non-thermally activated clays in the production of geopolymers, in: Provis, J.L., Van Deventer, J.S.J. (Eds.), Geopolymers: Structure, Processing, Properties and Industrial Applications, pp. 296-316.
Madejova, J., Komadel, P., 2001. Baseline studies of the clay minerals society source clays: infrared methods. Clays and Clay Minerals 49, 410-432.
Marom, G., Fischer, S., Tuler, F.R., Wagner, H.D., 1978. Hybrid effects in composites: conditions for positive or negative effects versus rule-of-mixtures behaviour. J Mater Sci 13, 1419-1426.
Marsh, A., Heath, A., Patureau, P., Evernden, M., Walker, P., 2018a. Alkali activation behaviour of un-calcined montmorillonite and illite clay minerals. Applied Clay Science 166, 250-261.
Marsh, A., Heath, A., Patureau, P., Evernden, M., Walker, P., 2018b. A mild conditions synthesis route to produce hydrosodalite from kaolinite, compatible with extrusion processing. Microporous and Mesoporous Materials 264, 125-132.
Maskell, D., Heath, A., Walker, P., 2013. Laboratory scale testing of extruded earth masonry units. Materials & Design 45, 359-364.
Mikuła, A., Król, M., Koleżyński, A., 2015. The influence of the long-range order on the vibrational spectra of structures based on sodalite cage. Spectrochimica Acta Part A: Molecular and Biomolecular Spectroscopy 144, 273-280.
Moloy, E.C., Liu, Q., Navrotsky, A., 2006. Formation and hydration enthalpies of the hydrosodalite family of materials. Microporous and Mesoporous Materials 88, 283-292.
Murmu, A.L., Patel, A., 2018. Towards sustainable bricks production: An overview. Construction and Building Materials 165, 112-125.
Murray, H.H., Keller, W.D., 1993. Kaolins, Kaolins and Kaolins, in: Murray, H.H., Bundy, W.M., Harvey, C.C. (Eds.), Kaolin Genesis and Utilization. Clay Minerals Society.
Nickovic, S., Vukovic, A., Vujadinovic, M., Djurdjevic, V., Pejanovic, G., 2012. High-resolution mineralogical database of dust-productive soils for atmospheric dust modeling. Atmospheric Chemistry and Physics 12, 845-855.
Omar Sore, S., Messan, A., Prud'homme, E., Escadeillas, G., Tsobnang, F., 2018. Stabilization of compressed earth blocks (CEBs) by geopolymer binder based on local materials from Burkina Faso. Construction and Building Materials 165, 333-345.
Pacheco-Torgal, F., Castro-Gomes, J., Jalali, S., 2008. Alkali-activated binders: A review. Part 2. About materials and binders manufacture. Construction and Building Materials 22, 1315-1322.
Provis, J.L., 2014. Geopolymers and other alkali activated materials: why, how, and what? Mat. Struct. 47, 11-25.
Prud'homme, E., Autef, A., Essaidi, N., Michaud, P., Samet, B., Joussein, E., Rossignol, S., 2013. Defining existence domains in geopolymers through their physicochemical properties. Applied Clay Science 73, 26-34.

Rees, C.A., Provis, J.L., Lukey, G.C., van Deventer, J.S.J., 2007a. Attenuated Total Reflectance Fourier Transform Infrared Analysis of Fly Ash Geopolymer Gel Aging. Langmuir 23, 8170-8179.
Rees, C.A., Provis, J.L., Lukey, G.C., van Deventer, J.S.J., 2007b. In Situ ATR-FTIR Study of the Early Stages of Fly Ash Geopolymer Gel Formation. Langmuir 23, 9076-9082.
Reeves, G.M., Sims, I., Cripps, J.C., 2006. Clay materials used in construction. Geological Society, London.
Richardson, C.K., Markuszewski, R., Durham, K.S., Bluhm, D.D., 1986. Effect of Caustic and Microwave Treatment on Clay Minerals Associated with Coal, Mineral Matter and Ash in Coal. American Chemical Society, pp. 513-523.
Roy, B.N., 1990. Infrared Spectroscopy of Lead and Alkaline-Earth Aluminosilicate Glasses. Journal of the American Ceramic Society 73, 846-855.
Seiffarth, T., Hohmann, M., Posern, K., Kaps, C., 2013. Effect of thermal pre-treatment conditions of common clays on the performance of clay-based geopolymeric binders. Applied Clay Science 73, 35-41.
Snellings, R., Mertens, G., Elsen, J., 2012. Supplementary Cementitious Materials. Reviews in Mineralogy and Geochemistry 74, 211-278.
Sperberga, I., Sedmale, G., Stinkulis, G., Zeila, K., Ulme, D., 2011. Comparative study of illite clay and illite-based geopolymer products, in: Niihara, K., Ohji, T., Sakka, Y. (Eds.), 3rd International Congress on Ceramics (ICC3). IOP Publishing, Osaka, Japan, p. 222027.
Tchadjie, L.N., Ekolu, S.O., 2018. Enhancing the reactivity of aluminosilicate materials toward geopolymer synthesis. J Mater Sci 53, 4709-4733.
Tchakoute, H.K., Rüscher, C.H., Djobo, J.N.Y., Kenne, B.B.D., Njopwouo, D., 2015. Influence of gibbsite and quartz in kaolin on the properties of metakaolin-based geopolymer cements. Applied Clay Science 107, 188-194.
Tironi, A., Trezza, M.A., Scian, A.N., Irassar, E.F., 2013. Assessment of pozzolanic activity of different calcined clays. Cement and Concrete Composites 37, 319-327.
Van der Marel, H.W., Beutelspacher, H., 1976. Atlas of infrared spectroscopy of clay minerals and their admixtures. Elsevier Scientific Publishing Company., Amsterdam; New York.
Wagner, J.F., 2013. Chapter 9 - Mechanical Properties of Clays and Clay Minerals, in: Bergaya, F., Lagaly, G. (Eds.), Handbook of Clay Science, 2nd ed. Elsevier, Amsterdam, pp. 347-381.
Weng, L., Sagoe-Crentsil, K., 2007. Dissolution processes, hydrolysis and condensation reactions during geopolymer synthesis: Part I—Low Si/Al ratio systems. J Mater Sci 42, 2997-3006.
Weng, L., Sagoe-Crentsil, K., Brown, T., Song, S., 2005. Effects of aluminates on the formation of geopolymers. Materials Science and Engineering: B 117, 163-168.
Xu, H., Van Deventer, J.S.J., 2000. The geopolymerisation of alumino-silicate minerals. International Journal of Mineral Processing 59, 247-266.
Zografou, A., 2015. The use of china clay waste as a construction material using alkali-activated cement technology. University of Bath.